Supporting Information for

Multifunctional MOFs-based Probes for Efficient Detection and Discrimination of Pb^{2+}, Fe^{3+} and $Cr_2O_7^{2-}/CrO_4^{2-}$

Fengqin Wang[a*], Fengxiao Zhang[b], Zhongrui Zhao[a], Zhenyu Sun[a], Yanyan Pu[b], Yanjun Wang[c], Xiaoqing Wang[c]

[a]*College of Chemistry, State Key Laboratory of Separation Membranes and Membrane Processes, Tiangong University, Tianjin, 300387, China*

[b]*College of Environmental Science and Engineering, Tiangong University, Tianjin, 300387, China*

[c]*College of Chemistry Engineering and Technology, Tiangong University, Tianjin, 300387, China*

E-mail address: wangfengqin@tiangong.edu.cn Tel: (+86)-22-83955458

Table S1 Crystal data and structure refinement for **Zn-MOF** and **Cd-MOF**

Compound	**Zn-MOF**	**Cd-MOF**
Chemical formula	$C_{26}H_{22}Zn_2N_2O_{14}S_2$	$C_{52}H_{36}Cd_4N_4O_{24}S_4$
Formula weight	781.32	1678.69
Temperature [K]	113(2)	113(2) K
Wavelength[Å]	0.71073	0.71073 A
Crystal system	Monoclinic	Monoclinic
Space group	P2(1)/c	C2/c
a[Å]	15.878(3)	14.862(4)
b[Å]	7.6402(15)	6.2811(13)
c[Å]	11.509(2)	28.213(6)
Volume [Å^3]	1389.9(5)	2619.8(11)
Z, Calculated density[Mg/m^3]	2, 1.867	2, 2.128
Absorption coefficient[mm^{-1}]	1.956	1.857
Crystal size[mm^3]	0.20×0.18×0.12	0.200 × 0.180 × 0.120
Theta range for data collection (deg)	2.58 to 25.02	1.451 to 27.744
Limiting indices	-18≤=h≤=18, -9≤=k≤=9, -13≤=l≤=13	-19<=h<=19, -8<=k<=8, -36<=l<=36
F(000)	792	1648
Reflections collected/unique	12693/2418 [R(int)=0.0434]	11489/3045 [R(int) = 0.0775]
Data/restraints/parameters	2418/18/223	3045/367/319
Goodness-of-fit on F^2	1.036	1.079
Final R indices[$I>2\sigma(I)$]	R_1 = 0.0442, wR_2 = 0.1085	R1 = 0.0556, wR2 = 0.1361
R indices (all data)	R_1 = 0.0486, wR_2 = 0.1116	R1 = 0.0768, wR2 = 0.1578
Largest diff. peak and hole[e.Å^{-3}]	1.165 and -0.472	1.321 and -1.455

Table S2 Selected bond lengths and angles for **Zn-MOF** and **Cd-MOF** (Å, º)

Zn-MOF			
Zn(1)-O(1)	1.950(3)	Zn(1)-O(4)#1	1.999(3)
Zn(1)-O(5)#2	2.023(3)	Zn(1)-O(7)	2.084(3)
Zn(1)-O(6)	2.103(3)		
O(1)-Zn(1)-O(4)#1	104.47(12)	O(1)-Zn(1)-O(5)#2	131.24(12)
O(4)#1-Zn(1)-O(7)	86.38(11)	O(5)#2-Zn(1)-O(7)	84.28(11)
O(1)-Zn(1)-O(6)	92.63(12)	O(4)#1-Zn(1)-O(6)	88.22(11)
O(5)#2-Zn(1)-O(6)	95.88(11)	O(7)-Zn(1)-O(6)	173.60(11)
O(4)#1-Zn(1)-O(5)#2	123.67(11)	O(1)-Zn(1)-O(7)	92.04(12)
Cd-MOF			
Cd(1)-O(5)#1	2.171(4)	Cd(1)-O(11)	2.247(4)
Cd(1)-O(2)	2.284(4)	Cd(1)-O(4)#2	2.324(4)
Cd(1)-O(1)#3	2.409(4)	Cd(1)-O(1)	2.488(4)
O(5)#1-Cd(1)-O(11)	98.84(15)	O(5)#1-Cd(1)-O(2)	120.54(15)
O(11)-Cd(1)-O(2)	140.43(14)	O(5)#1-Cd(1)-O(4)#2	96.59(17)
O(11)-Cd(1)-O(4)#2	85.54(15)	O(2)-Cd(1)-O(4)#2	86.28(15)
O(5)#1-Cd(1)-O(1)#3	87.90(16)	O(11)-Cd(1)-O(1)#3	85.12(14)
O(2)-Cd(1)-O(1)#3	99.01(14)	O(4)#2-Cd(1)-O(1)#3	170.16(13)
O(5)#1-Cd(1)-O(1)	162.56(17)	O(11)-Cd(1)-O(1)	88.29(13)
O(2)-Cd(1)-O(1)	55.24(12)	O(4)#2-Cd(1)-O(1)	99.83(15)
O(1)#3-Cd(1)-O(1)	76.81(15)		

Symmetry transformations used to generate equivalent atoms:

For **Zn-MOF**:

#1 -x, y-1/2, -z+3/2 #2 x+1, -y+1/2, z+1/2 #3 -x, y+1/2, -z+3/2

For **Cd-MOF**:

#1 x+1/2, -y+1/2, z-1/2 #2 -x+1/2, y+1/2, -z+1/2 #3 -x+1/2, -y+3/2, -z

Table S3 The comparisons between the characteristic emission of Eu^{3+} and the ligand-based emission in Eu^{3+}@MOFs

Substrates	Eu^{3+}@**Zn-MOF**			Eu^{3+}@**Cd-MOF**		
	Quenching efficiency		Eu/L	Quenching efficiency		Eu/L
	Eu (based on 617 nm)	L (based on 455 nm)		Eu (based on 617 nm)	L (based on 461 nm)	
$Cr_2O_7^{2-}$	91.35%	86.63%	1.06	92.50%	94.24%	0.98
CrO_4^{2-}	91.98%	75.89%	1.21	95.69%	90.71%	1.06
Fe^{3+}	67.09%	64.71%	1.04	57.00%	48.42%	1.18

Table S4 The corresponding comparisons of K_{sv} and LOD for MOFs and Eu^{3+}@MOFs

Substrates		**Zn-MOF**	Eu^{3+}@**Zn-MOF**	**Cd-MOF**	Eu^{3+}@**Cd-MOF**
$Cr_2O_7^{2-}$	K_{sv}	1.11×10^4	4.87×10^3	8.47×10^3	5.02×10^3
	LOD (μM)	43	62	71	72
	Ratio of K_{sv}		2.28		1.69
CrO_4^{2-}	K_{sv}	1.07×10^4	5.01×10^3	1.96×10^4	7.54×10^3
	LOD (μM)	45	60	31	47
	Ratio of K_{sv}		2.13		2.60
Fe^{3+}	K_{sv}	1.69×10^4	1.88×10^3	1.04×10^4	1.63×10^3
	LOD (μM)	28	159	57	221
	Ratio of K_{sv}		8.99		6.40
Pb^{2+}	K_{sv}	0.80×10^3	0.08×10	1.88×10^3	0.02×10^3
	LOD (μM)	600	/	370	/
	Ratio of K_{sv}		10.00		94.00

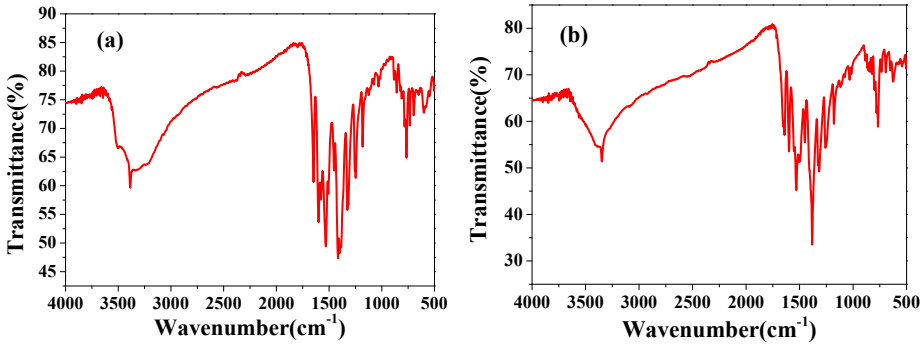

Fig. S1 FT-IR spectra of (a) **Zn-MOF**; (b) **Cd-MOF**.

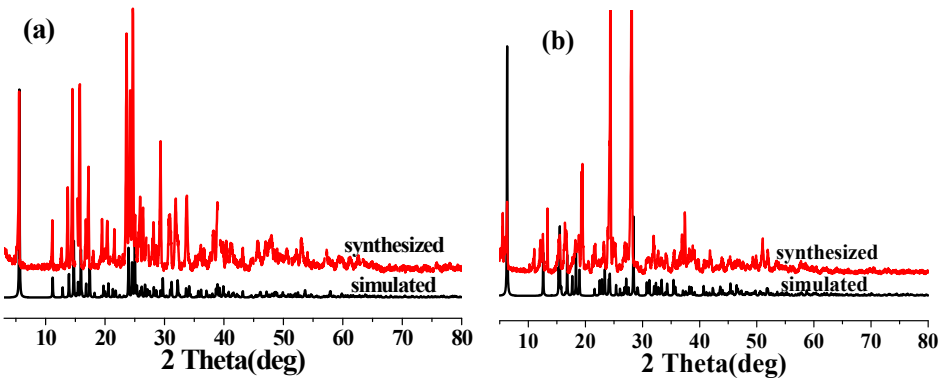

Fig. S2 PXRD patterns of (a) **Zn-MOF**; (b) **Cd-MOF**.

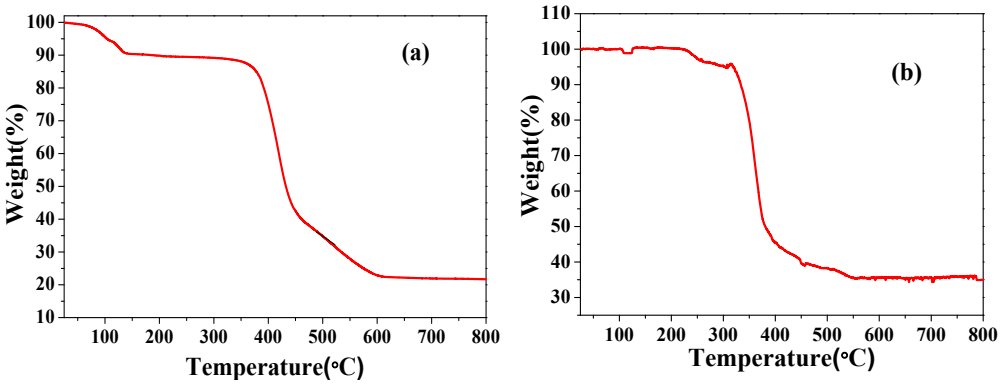

Fig. S3 TG curve of (a) **Zn-MOF**; (b) **Cd-MOF** in Ar condition.

Element	*Wt%*	*At%*
CK	35.56	60.35
NK	02.88	04.19
OK	16.52	21.04
SK	11.73	07.46
EuL	19.32	02.59
ZnK	14.00	04.36
Matrix	Correction	ZAF

Element	*Wt%*	*At%*
CK	48.41	65.11
NK	05.00	05.77
OK	24.06	24.29
SK	05.67	02.86
CdL	05.12	00.74
EuL	11.75	01.25
Matrix	Correction	ZAF

Fig. S4 The EDX results of Eu^{3+}@**Zn-MOF** and Eu^{3+}@**Cd-MOF**.

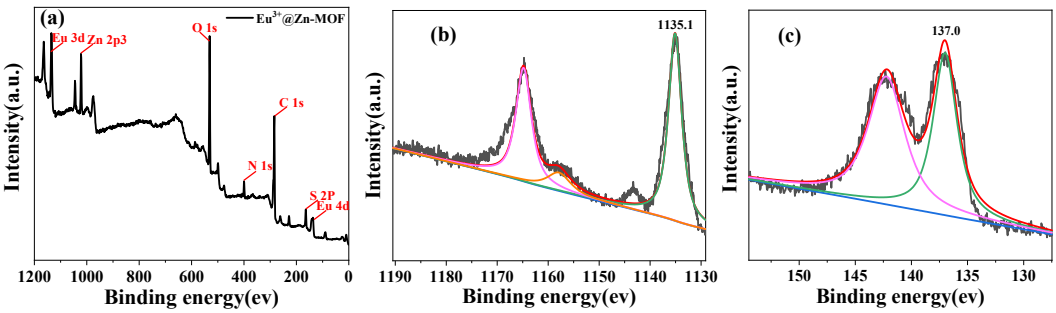

Fig. S5 (a) The XPS spectrum of Eu^{3+}@**Zn-MOF**; (b) Eu 3d XPS spectrum of Eu^{3+}@ **Zn-MOF**; (c) Eu 4d XPS spectrum of Eu^{3+}@ **Zn-MOF**.

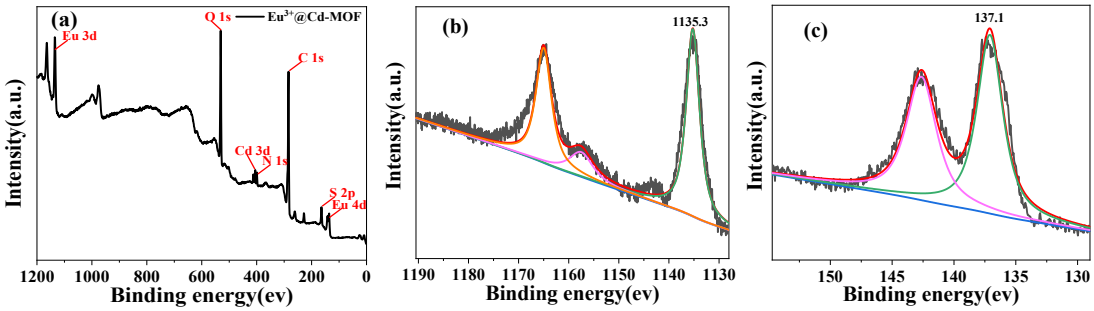

Fig. S6 (a) The XPS spectrum of Eu^{3+}@**Cd-MOF**; (b) Eu 3d XPS spectrum of Eu^{3+}@ **Cd-MOF**; (c) Eu 4d XPS spectrum of Eu^{3+}@ **Cd-MOF**.

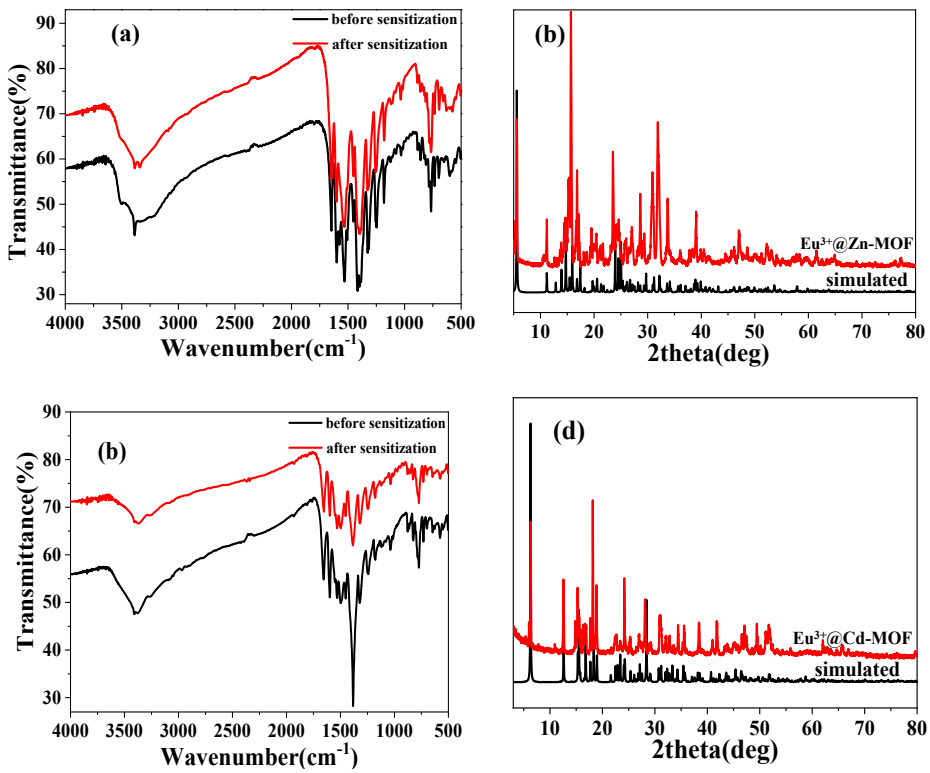

Fig. S7 The FT-IR spectra and powder X-ray diffraction of Eu^{3+}@MOFs before and after sensitization. (a), (b) Eu^{3+}@**Zn-MOF**; (c), (d) Eu^{3+}@**Cd-MOF**.

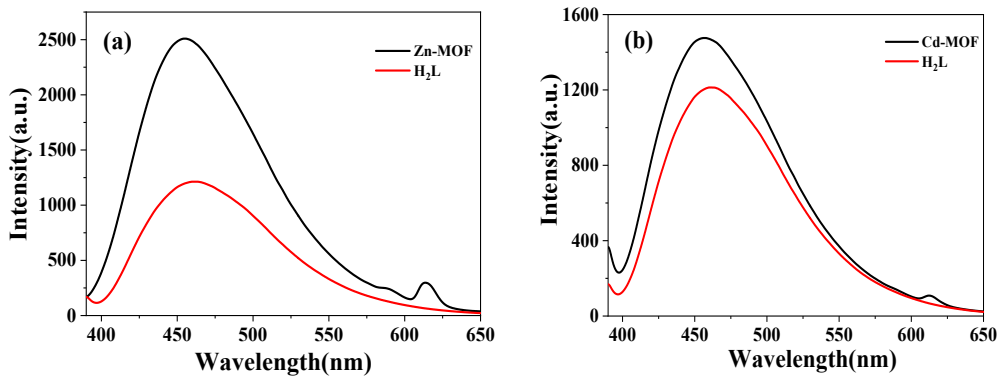

Fig. S8 The solid state fluorescence emission spectra of (a) **Zn-MOF**; (b) **Cd-MOF**.

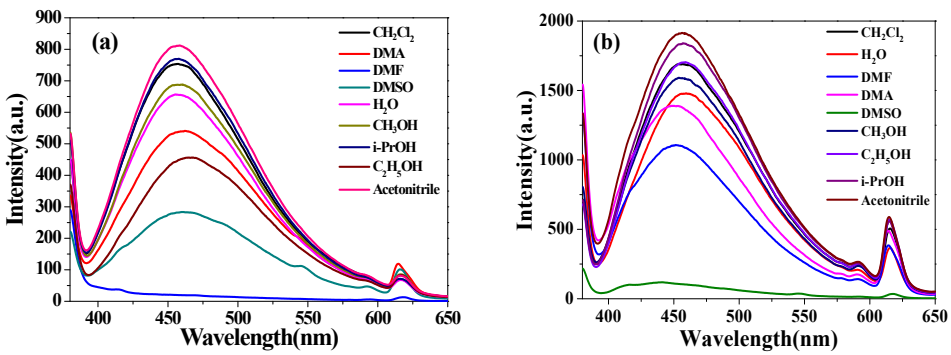

Fig. S9 The fluorescence emission spectra of (a) **Zn-MOF**; (b) **Cd-MOF** in different solvents at room temperature.

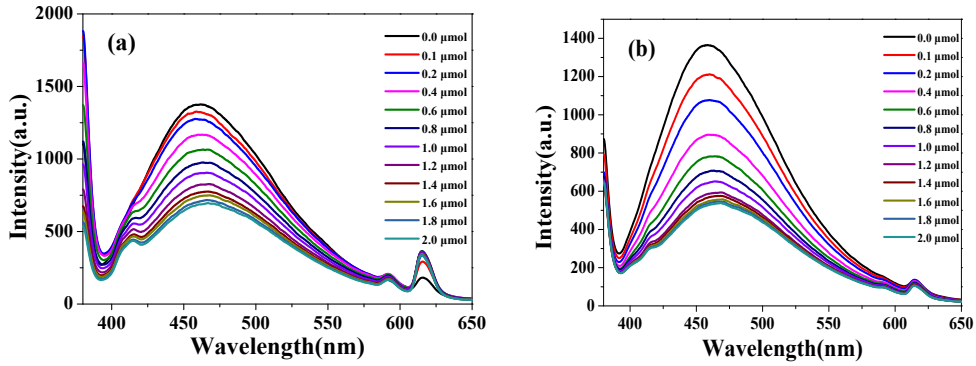

Fig. S10 Fluorescence titration of (a) **Zn-MOF**; (b) **Cd-MOF** dispersed in aqueous solution with the addition of different amount of 10^{-2} M aqueous solution of Pb^{2+}.

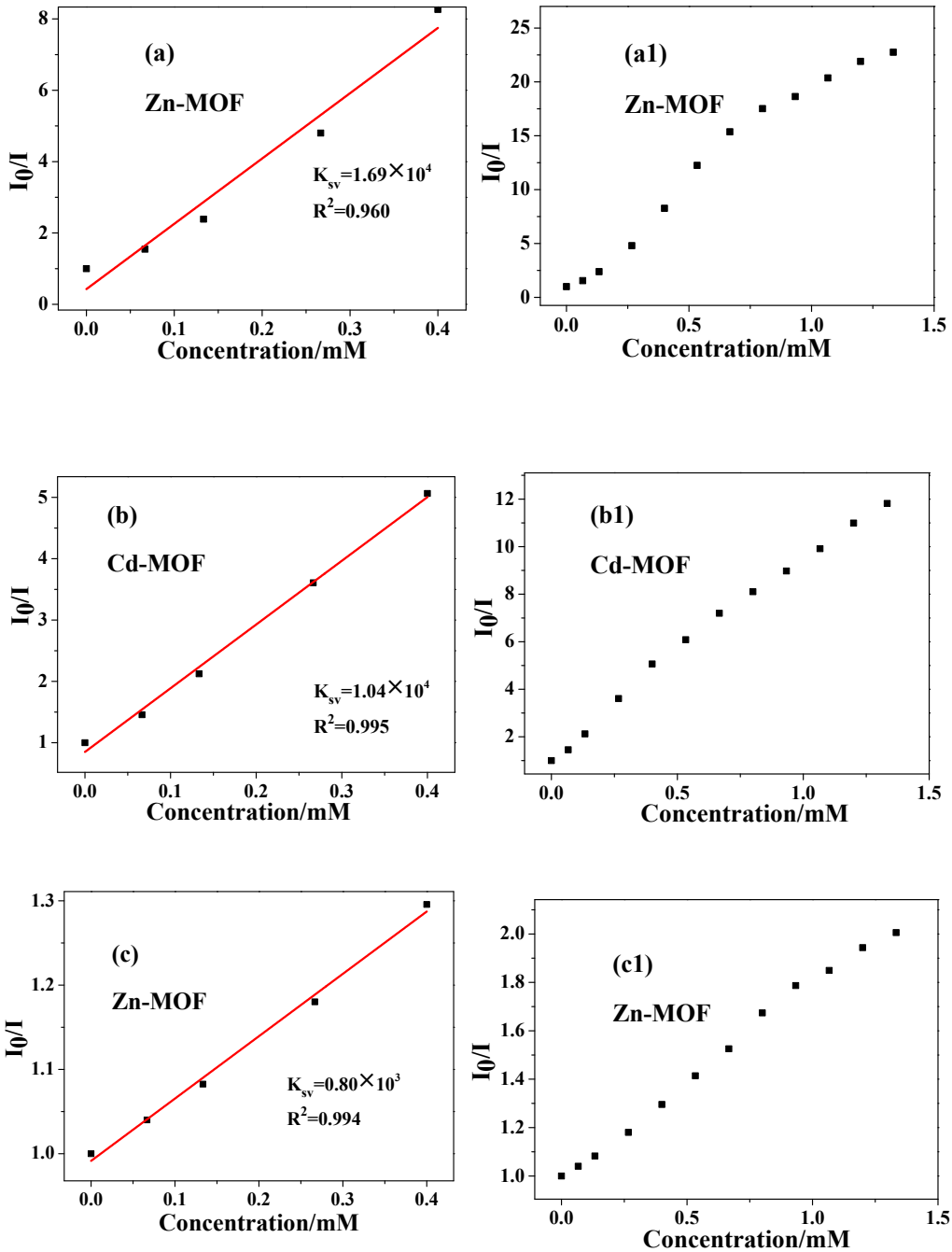

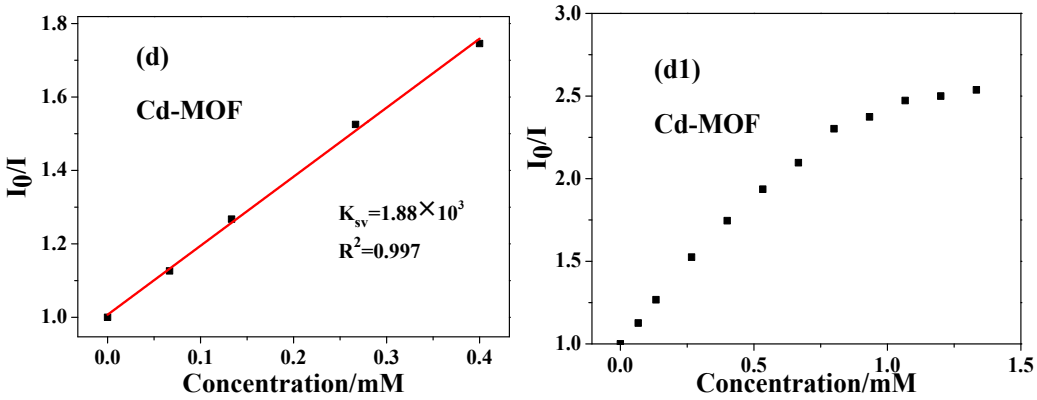

Fig. S11 Stern–Volmer plots of MOFs for Fe^{3+} and Pb^{2+} in low concentration region (a) **Zn-MOF**, (b) **Cd-MOF** for Fe^{3+}; c) **Zn-MOF**, d) **Cd-MOF** for Pb^{2+} respectively and (a1)-(d1) is the corresponding Stern–Volmer plots in full concentration region.

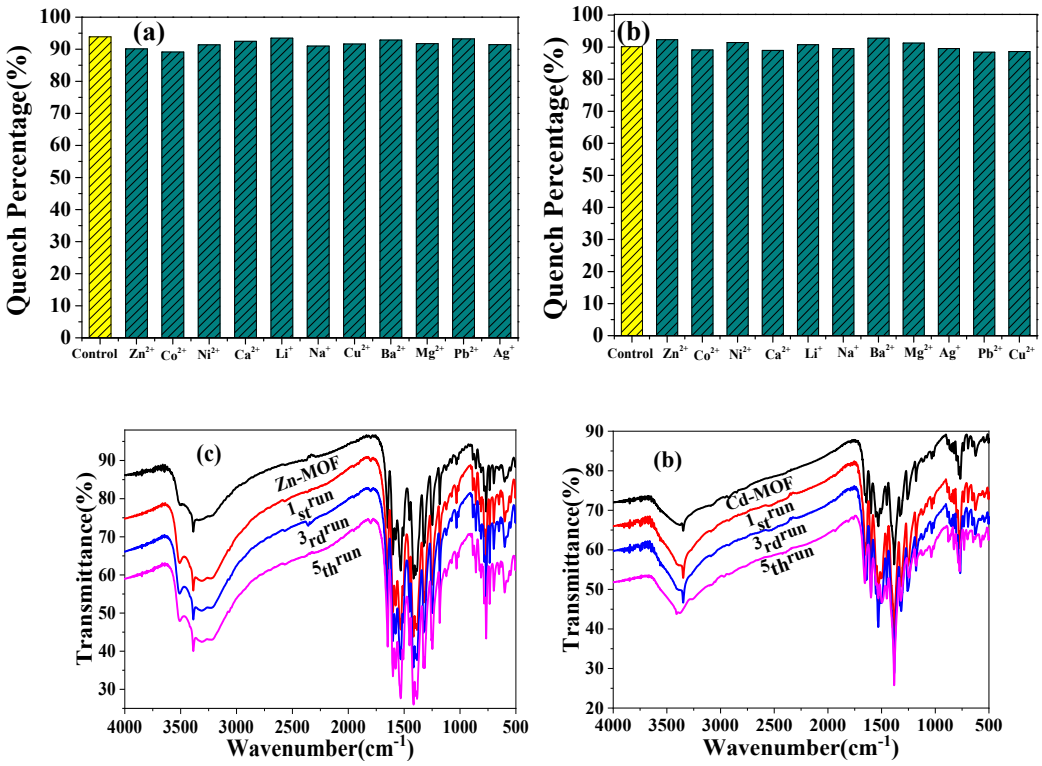

Fig. S12 Competitive binding studies of the different metal ions on (a) **Zn-MOF**; (b) **Cd-MOF** in aqueous solution. Yellow bar represents the quenching efficiency of MOFs with the addition of 2 umol (10^{-2} M, 200μL) Fe^{3+}. Blue bar represents the quenching efficiency of MOFs with the addition of 2 umol (10^{-2} M, 200μL) Fe^{3+} and 1 umol (10^{-2} M, 100μL) other metal ions. And the IR of MOFs for Fe^{3+} before and after the fluorescence sensing. (c) **Zn-MOF**; (d) **Cd-MOF**.

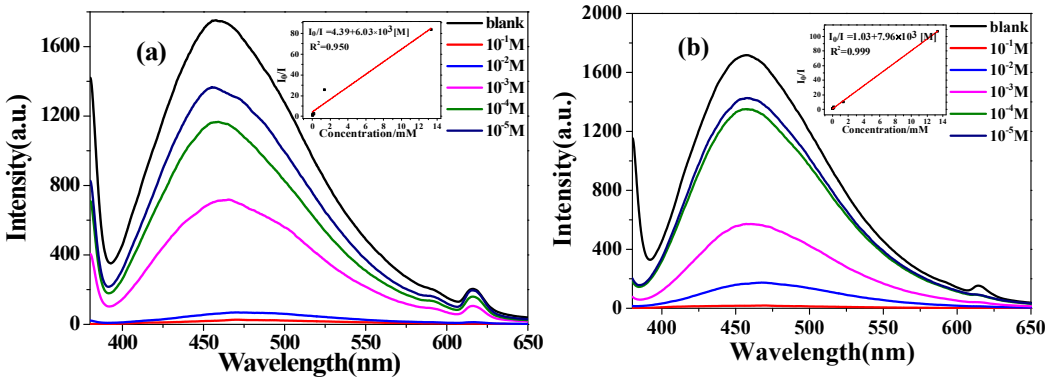

Fig. S13 The fluorescence spectra of (a) **Zn-MOF**; (b) **Cd-MOF** with the addition of different concentrations of 10^{-5} M to 10^{-1} M aqueous solution of Fe^{3+}. The insert is Stern-Volmer plot of (a) **Zn-MOF**; (b) **Cd-MOF** quenched by Fe^{3+} in aqueous solution.

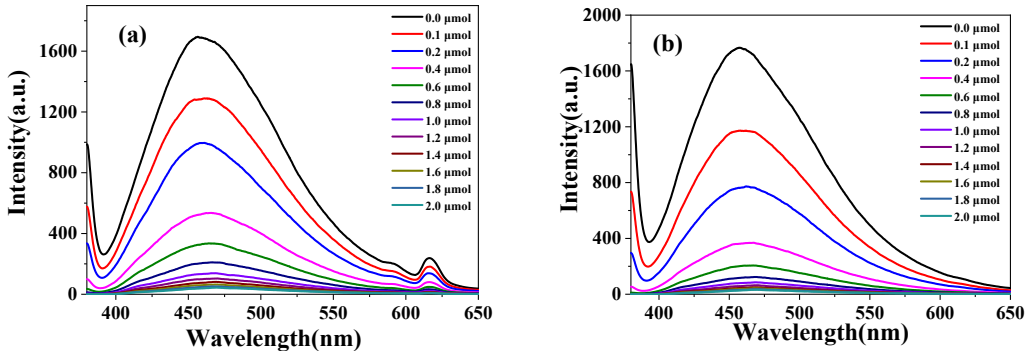

Fig. S14 Fluorescence titration of (a) **Zn-MOF**; (b) **Cd-MOF** dispersed in aqueous solution with the addition of different amount of 10^{-2} M aqueous solution of CrO_4^{2-}.

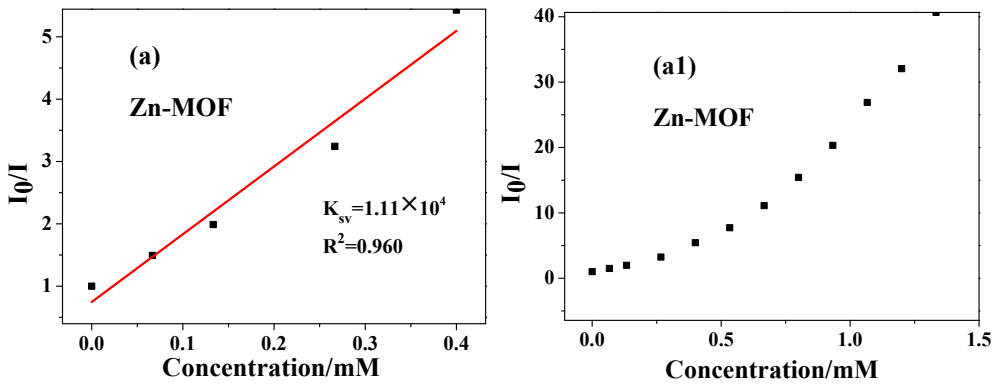

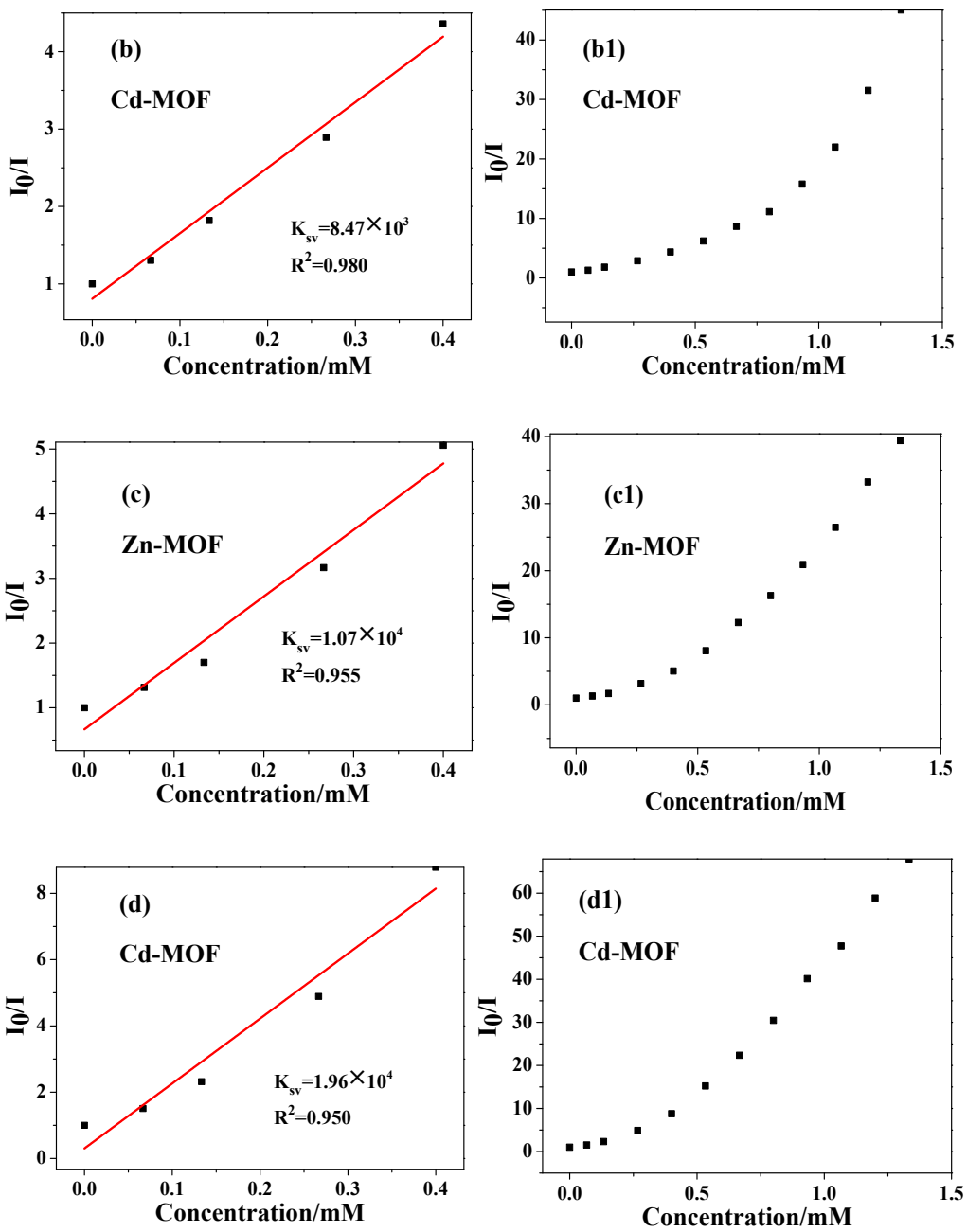

Fig. S15 Stern–Volmer plots of MOFs for $Cr_2O_7^{2-}$ and CrO_4^{2-} in low concentration region (a) **Zn-MOF**, (b) **Cd-MOF** for $Cr_2O_7^{2-}$; c) **Zn-MOF**, d) **Cd-MOF** for CrO_4^{2-} respectively and (a1)-(d1) is the corresponding Stern–Volmer plots in full concentration region.

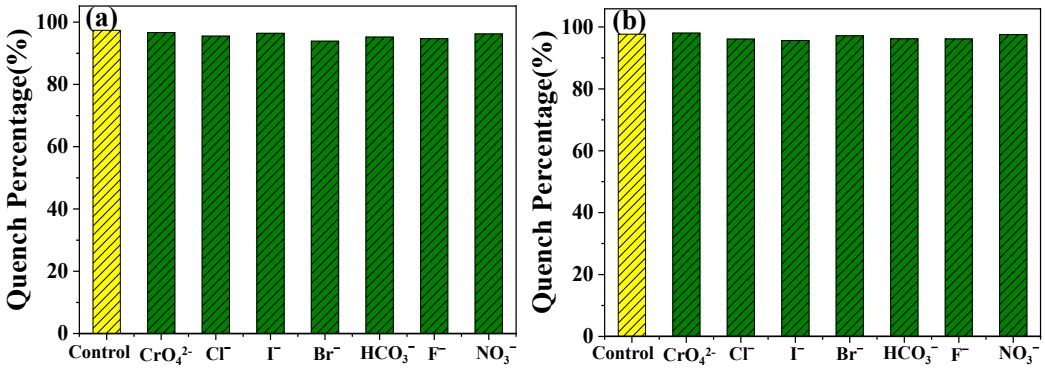

Fig. S16 Competitive binding studies of the different anions (10^{-2} M, 100 μL) on (a) **Zn-MOF**; (b) **Cd-MOF** to $Cr_2O_7^{2-}$ in aqueous solution.

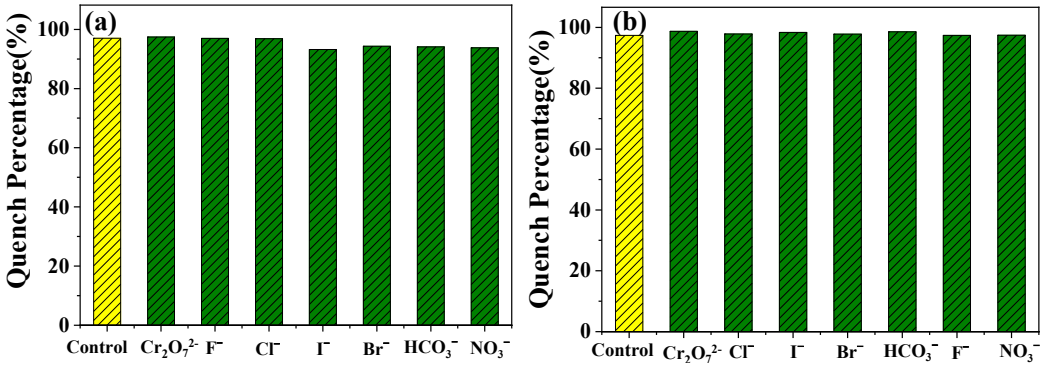

Fig. S17 Competitive binding studies of the different anions (10^{-2} M, 100 μL) on (a) **Zn-MOF**; (b) **Cd-MOF** to CrO_4^{2-} in aqueous solution.

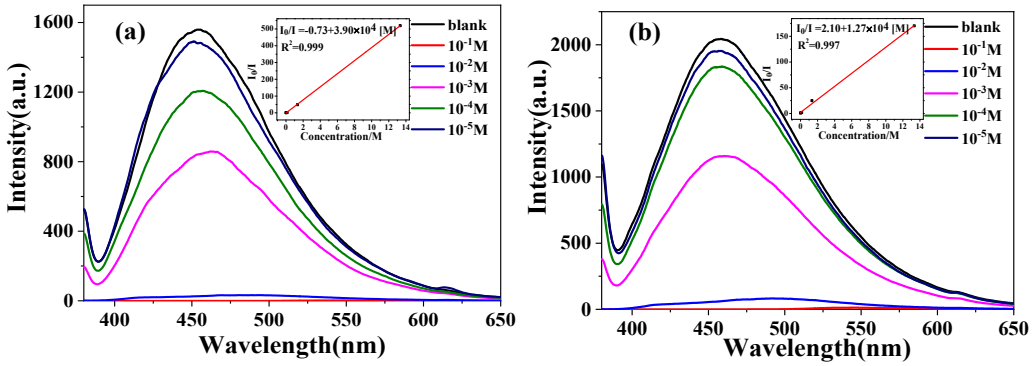

Fig. S18 The fluorescence spectra of (a) **Zn-MOF**; (b) **Cd-MOF** with the addition of different concentrations of 10^{-5} M to 10^{-1} M aqueous solution of $Cr_2O_7^{2-}$. The insert is Stern-Volmer plot of **Zn-MOF** and **Cd-MOF** quenched by $Cr_2O_7^{2-}$ in aqueous solution.

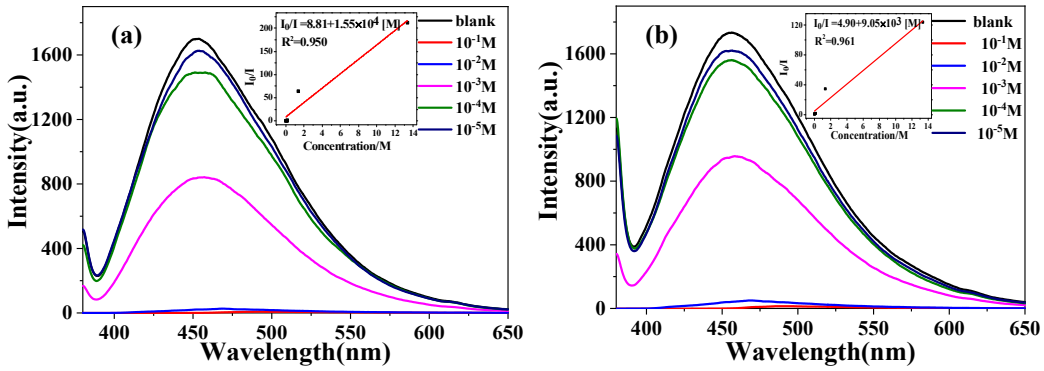

Fig. S19 The fluorescence spectra of (a) **Zn-MOF**; (b) **Cd-MOF** with the addition of different concentrations of 10^{-5} M to 10^{-1} M aqueous solution of CrO_4^{2-}. The insert is Stern-Volmer plot of **Zn-MOF** and **Cd-MOF** quenched by CrO_4^{2-} in aqueous solution.

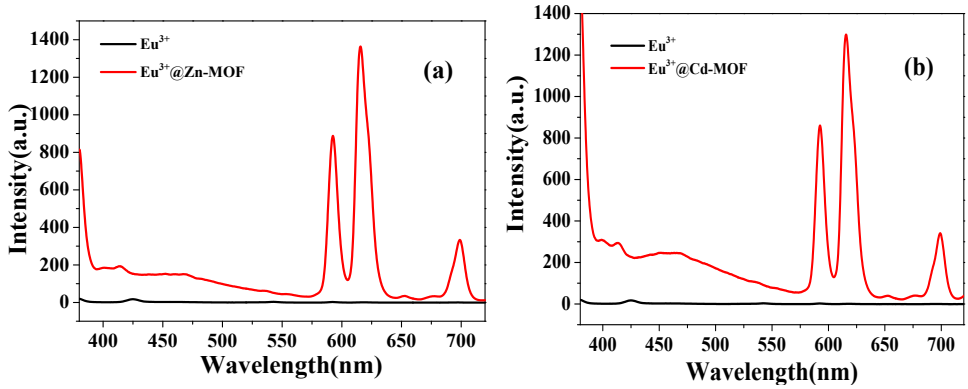

Fig. S20 The fluorescence spectra of (a) Eu^{3+}@**Zn-MOF**; (b) Eu^{3+}@**Cd-MOF** and free Eu^{3+} in aqueous solution.

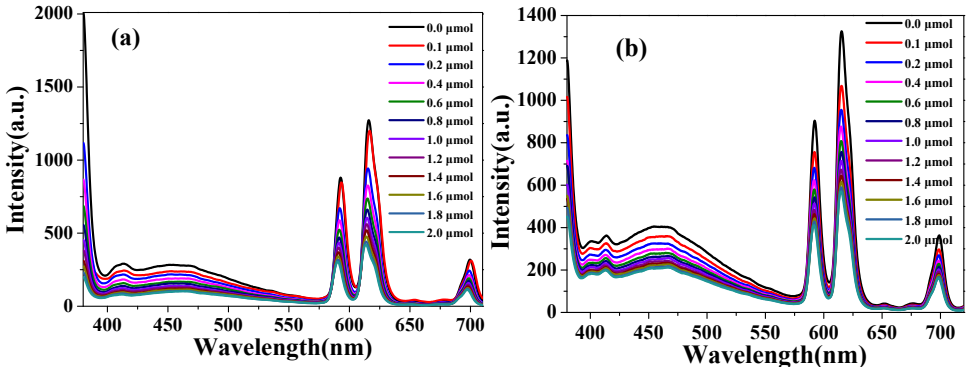

Fig. S21 Fluorescence titration of (a) Eu^{3+}@**Zn-MOF**; (b) Eu^{3+}@**Cd-MOF** dispersed in aqueous solution with the addition of different amount of 10^{-2} M aqueous solution of Fe^{3+}.

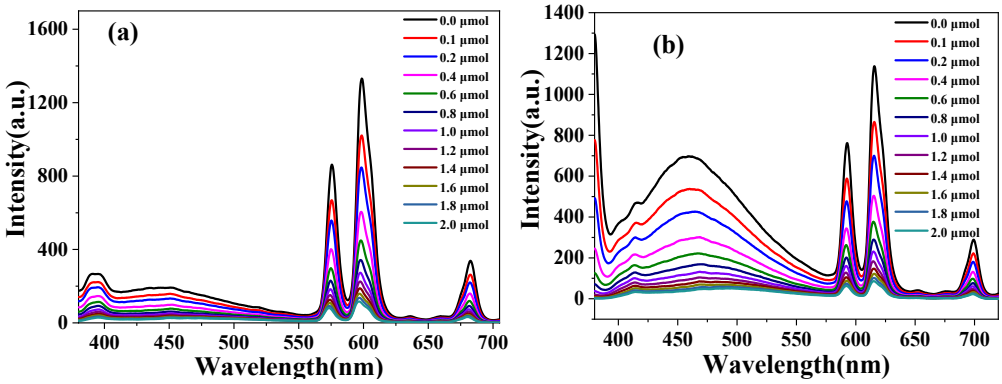

Fig. S22 Fluorescence titration of (a) Eu^{3+}@**Zn-MOF**; (b) Eu^{3+}@**Cd-MOF** dispersed in aqueous solution with the addition of different amount of 10^{-2} M aqueous solution of $Cr_2O_7^{2-}$.

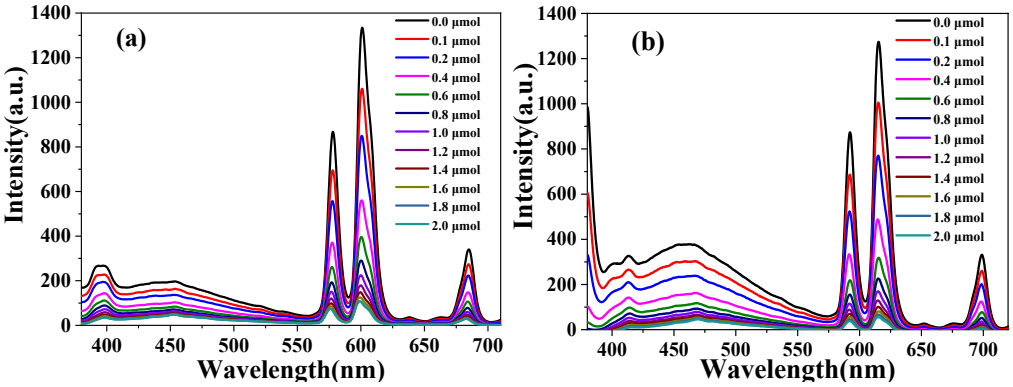

Fig. S23 Fluorescence titration of (a) Eu^{3+}@**Zn-MOF**; (b) Eu^{3+}@**Cd-MOF** dispersed in aqueous solution with the addition of different amount of 10^{-2} M aqueous solution of CrO_4^{2-}.

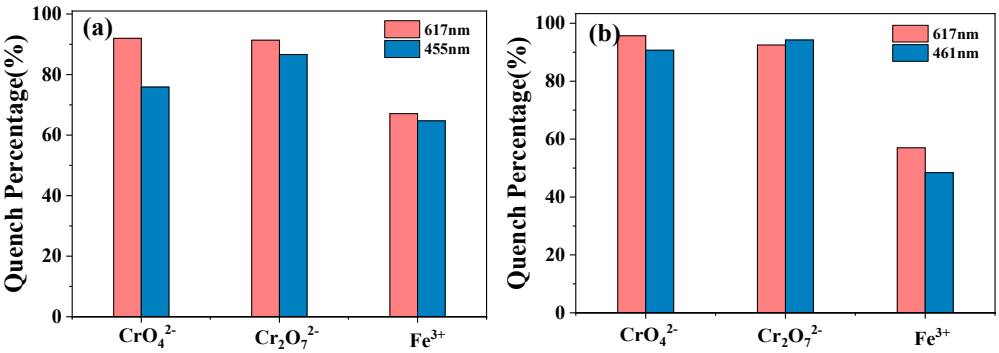

Fig. S24 The percentage of fluorescence quenching at 617nm and 455nm, 461nm of Eu^{3+}@MOFs obtained for different cation and anions (10^{-2} M) in aqueous solution at room temperature. (a) **Eu^{3+}@Zn-MOF**; (b) **Eu^{3+}@Cd-MOF**.

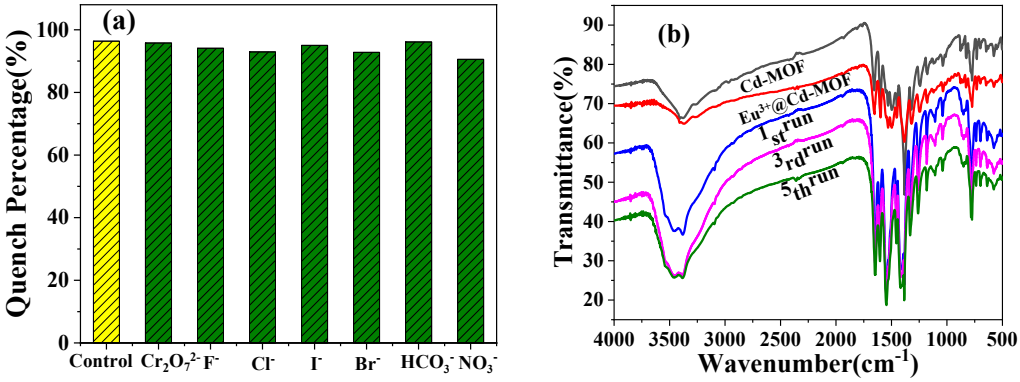

Fig. S25 Competitive binding studies of the different anions (10^{-2} M, 100 μL) Eu^{3+}@**Cd-MOF** to CrO_4^{2-} in aqueous solution. And the IR spectra of Eu^{3+}@**Cd-MOF** for CrO_4^{2-} before and after the fluorescence sensing.

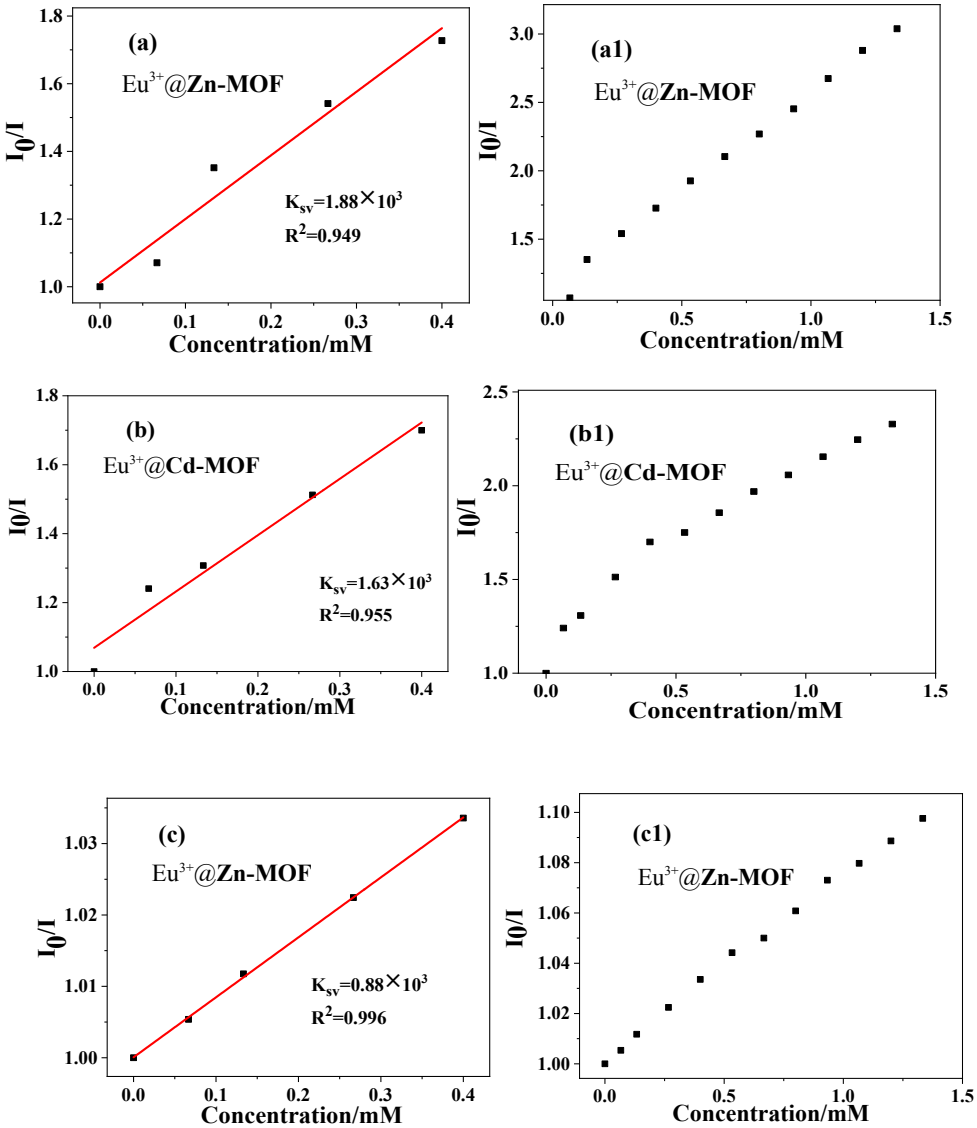

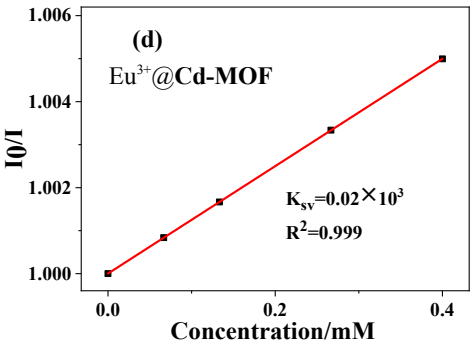
(d)
Eu3+@Cd-MOF
Ksv=0.02×10^3
R2=0.999
I0/I
Concentration/mM

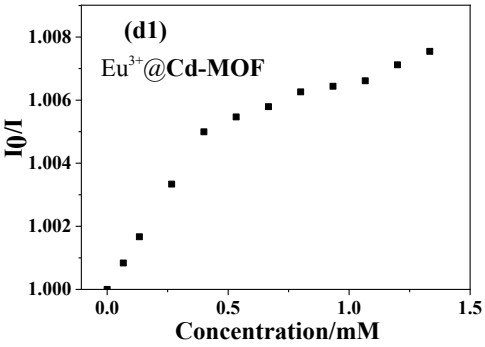
(d1)
Eu3+@Cd-MOF
I0/I
Concentration/mM

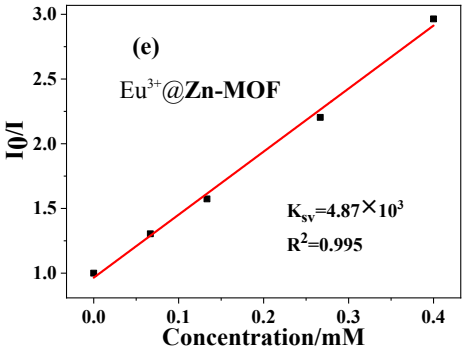
(e)
Eu3+@Zn-MOF
Ksv=4.87×10^3
R2=0.995
I0/I
Concentration/mM

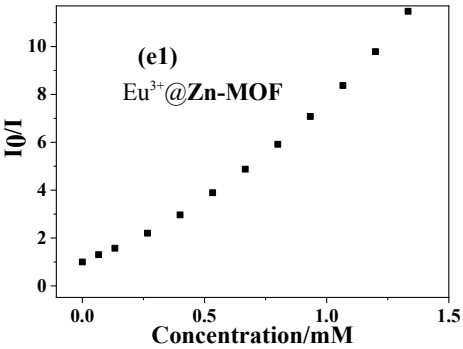
(e1)
Eu3+@Zn-MOF
I0/I
Concentration/mM

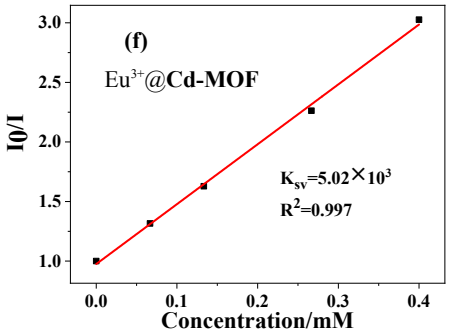
(f)
Eu3+@Cd-MOF
Ksv=5.02×10^3
R2=0.997
I0/I
Concentration/mM

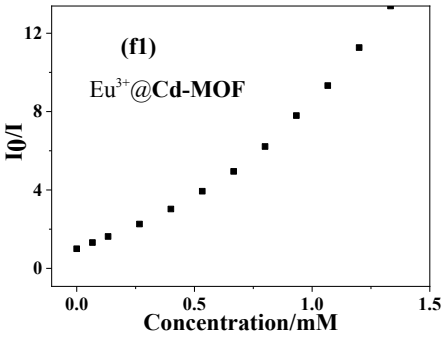
(f1)
Eu3+@Cd-MOF
I0/I
Concentration/mM

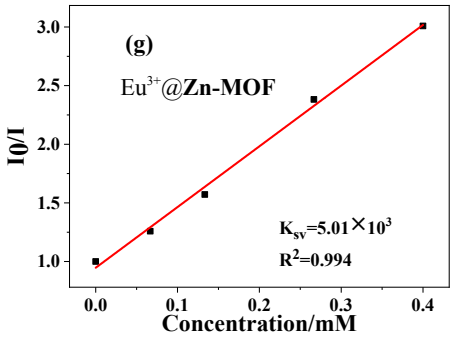
(g)
Eu3+@Zn-MOF
Ksv=5.01×10^3
R2=0.994
I0/I
Concentration/mM

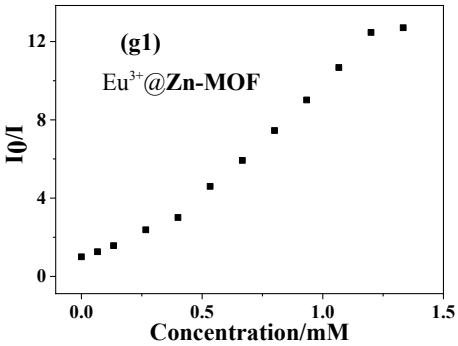
(g1)
Eu3+@Zn-MOF
I0/I
Concentration/mM

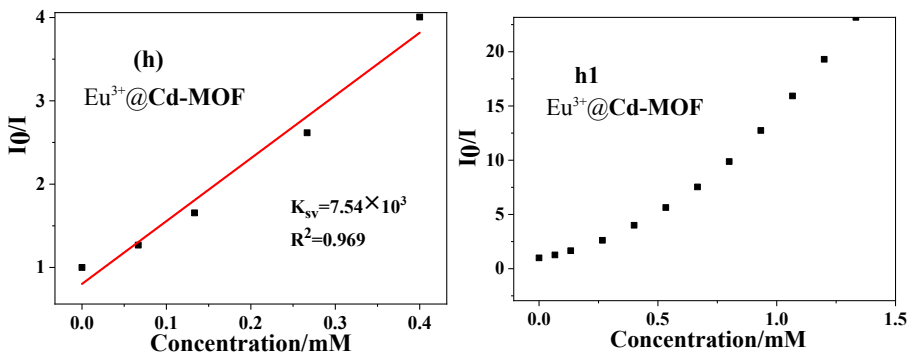

Fig. S26 Stern–Volmer plots of Eu^{3+}@MOFs for Fe^{3+}; Pb^{2+}; $Cr_2O_7^{2-}$ and CrO_4^{2-} in low concentration region (a) Eu^{3+}@**Zn-MOF**, (b) Eu^{3+}@**Cd-MOF** for Fe^{3+}, respectively; (c) Eu^{3+}@**Zn-MOF**, d) Eu^{3+}@**Cd-MOF** for Pb^{2+}, respectively; (e) Eu^{3+}@**Zn-MOF**, (f) Eu^{3+}@**Cd-MOF** for $Cr_2O_7^{2-}$, respectively; (g) Eu^{3+}@**Zn-MOF**, (h) Eu^{3+}@**Cd-MOF** for CrO_4^{2-} respectively; (a1)-(h1) is the corresponding Stern–Volmer plots in full concentration region.

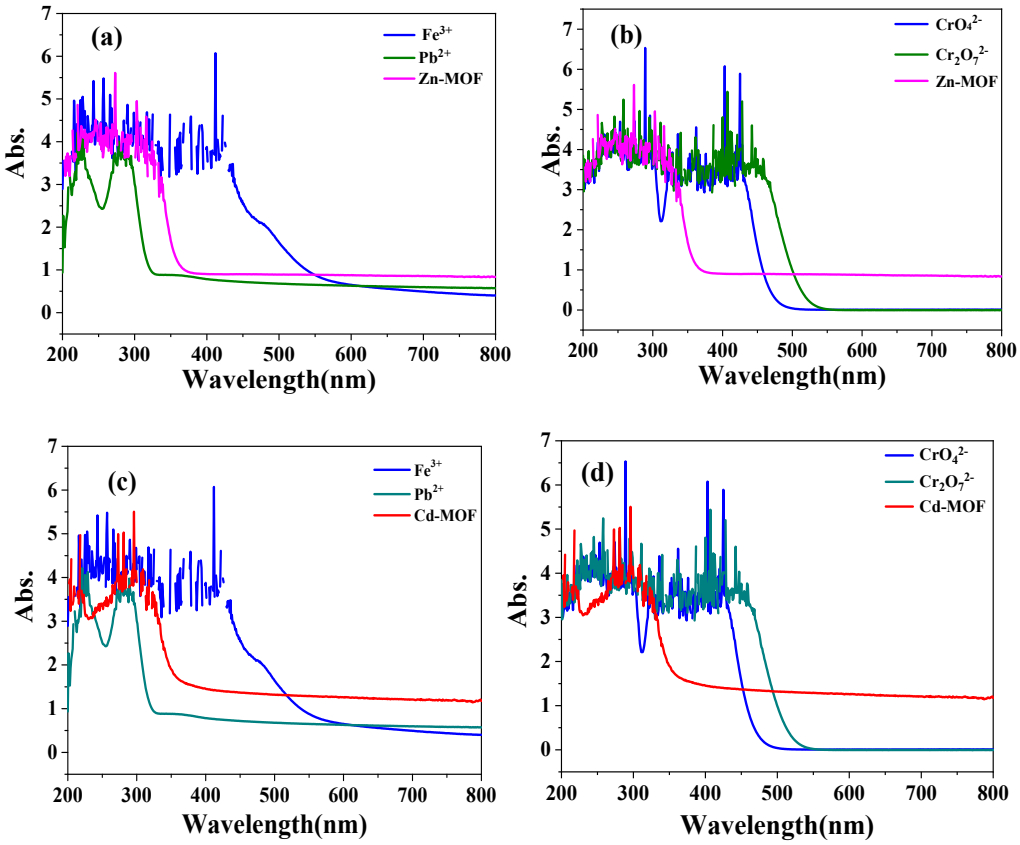

Fig. S27 The liquid UV-vis spectra of MOFs upon addition of Fe^{3+}, Pb^{2+}, CrO_4^{2-} and $Cr_2O_7^{2-}$ in practical concentration.

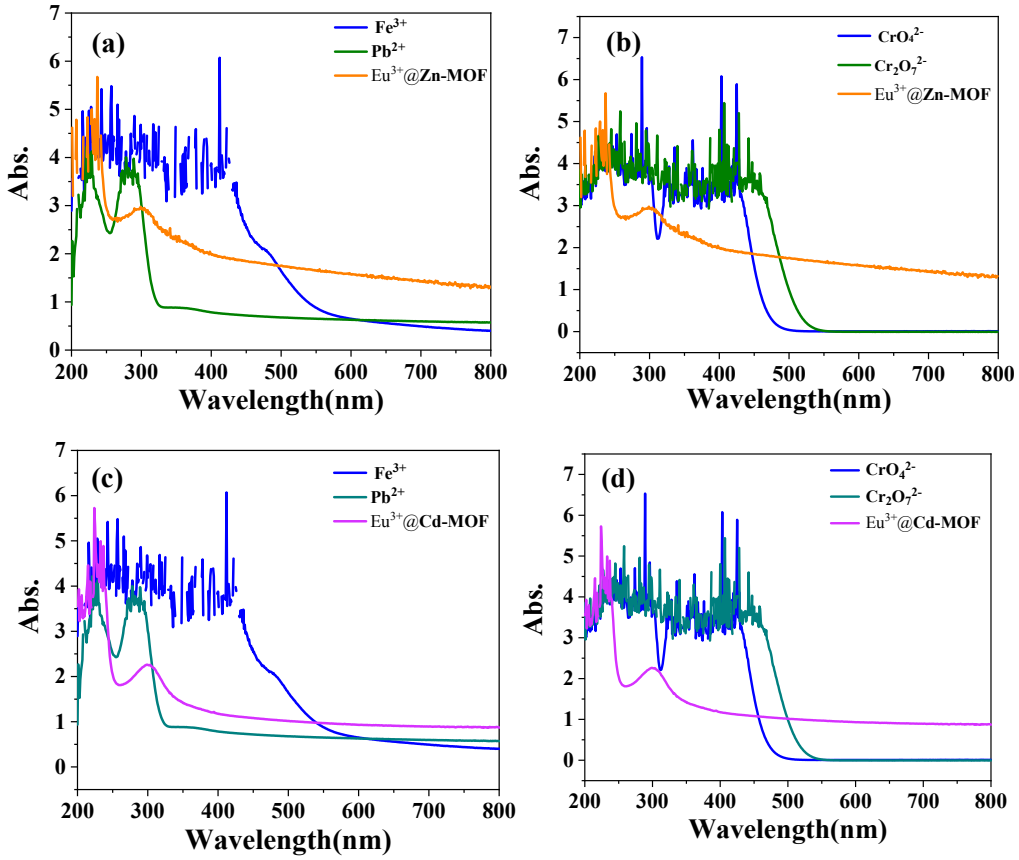

Fig. S28 The liquid UV-vis spectra of Eu^{3+}@MOFs upon addition of Fe^{3+}, Pb^{2+}, CrO_4^{2-} and $Cr_2O_7^{2-}$ in practical concentration.